
Graph Intervention Networks for Causal Effect Estimation

Jean Kaddour*

Centre for Artificial Intelligence
University College London

Qi Liu

Department of Computer Science
University of Oxford

Yuchen Zhu

Centre for Artificial Intelligence
University College London

Matt J. Kusner

Centre for Artificial Intelligence
University College London

Ricardo Silva

Department of Statistical Science
University College London

Abstract

We address the estimation of conditional average treatment effects (CATEs) when treatments are graph-structured (e.g., molecular graphs of drugs). Given a weak condition on the effect, we propose a plug-in estimator that decomposes CATE estimation into separate, simpler optimization problems. Our estimator (a) isolates the causal estimands (reducing regularization bias), and (b) allows one to plug in arbitrary models for learning. In experiments with small-world and molecular graphs, we show that our approach outperforms prior approaches and is robust to varying selection biases. Our implementation is online².

1 Introduction

Estimating covariate-level causal effects, so-called *conditional average treatment effects* (CATEs), from observational data is a fundamental problem across many domains. Examples include understanding the effects of non-pharmaceutical interventions on the transmission of COVID-19 in a specific region [13], on whether school meal programs improve child health [14], and the effects of chemotherapy drugs on cancer patients [52]. Supervised learning methods face two challenges in such settings: (i) *missing counterfactuals*, the fact that we only observe one treatment for each unit means models must extrapolate to new treatments without access to ground truth, and (ii) *confounding factors* that affect both treatment assignment and the outcome means that extrapolation from observation to intervention requires assumptions. Many approaches have been proposed to overcome these issues [1, 2, 3, 4, 5, 6, 7, 10, 11, 17, 20, 21, 23, 24, 25, 27, 29, 31, 35, 40, 42, 43, 45, 52, 56, 57, 61, 65, 68].

In many cases, treatments are naturally represented as graphs: the spatial network of regional transmission, the nutritional content of meals, and molecular structure of chemotherapy drugs. However, the vast majority of prior work operates with categorical (mostly binary) or continuous scalar treatments – we describe a notable exception [18] in Section 2. Adapting these methods is problematic: even if one was willing to suffer the exponential increases in runtime and/or memory, they would still not leverage the structure of graph data.

*Correspondence to jean.kaddour.20@ucl.ac.uk

²<https://github.com/JeanKaddour/GIN>

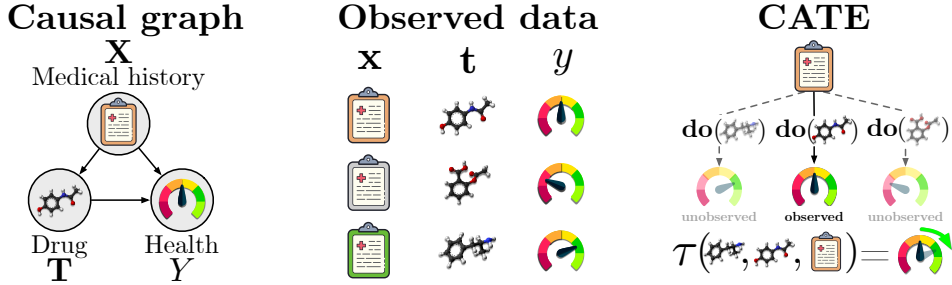


Figure 1: **Pictorial depiction for CATE estimation with graph interventions.** *Left:* Causal graph of problem setup with covariates X , treatment T , and outcome Y . *Center:* Observational data the estimator has access to, typically containing only one outcome per unit. *Right:* the CATE is defined as the difference between the expected outcomes given a fixed unit and a pair of treatments.

In this work, we propose *Graph Intervention Networks* (GIN), a CATE estimation method designed for *graph interventions*. Concretely, our contributions are:

- Given a weak condition on the structural form of the outcomes (Assumption 3), we generalize a well-known decomposition of CATE estimation [47] to graph treatments³.
- This decomposition reveals a learnable pseudo-outcome target that isolates the causal component of the observed signal by partialling out confounding associations. To derive it, we introduce a generic variation of the propensity score idea [48], which we term *propensity features*.
- Our method allows one to plug in any supervised learning methods for learning nuisance and target functions. We extend recent work on *plug-in estimators* [31] focusing on binary treatments to graph-structured treatments and integrating representation learning into CATE estimation.
- We show in experiments with small-world networks and molecular graphs that previous approaches can learn causal effects sub-optimally. In contrast, GIN successfully estimates these effects and is robust to varying levels of confounding.

2 Related Work

Graph interventions. Closest to our work is GraphITE [18], a method that learns representations of graph interventions for CATE estimation. They propose to minimize prediction loss plus a regularization term that aims to control for confounding based on the Hilbert-Schmidt Independence Criterion (HSIC) [16]. This technique suffers from two drawbacks: (i) $\mathcal{O}(b^2)$ scaling: the HSIC requires multiplication of kernel matrices and so scales quadratically in the batch size b , for each optimization step; (ii) *Hyper-parameter selection*: The HSIC term is multiplied by a weight λ ; a hyper-parameter which controls the trade-off between minimizing loss and confounding. However, it is unclear how to select this hyper-parameter, as ground-truth CATEs are never observed, and empirical loss does not bound CATE estimation error [1, 43, 54].

Plug-in estimators. A recent line of work for CATE estimation derives *plug-in estimators*⁴ [9]. These work by decomposing CATE estimation into multiple sub-problems (so-called *nuisance components*), each solvable using any supervised learning method [11, 17, 28, 31, 43]. Currently, these approaches are limited to binary treatment setups. Our approach is inspired by these methods, extending plug-in estimation to graph treatment settings.

CATE estimation with neural networks. Neural network CATE estimators typically use separate prediction heads for each treatment option [26, 34, 42, 51, 52, 54, 55]. This architectural design reduces one source of regularization bias: the influence of the treatment indicator variable might be lost in the high-dimensional network representations. Extending this idea directly to graph-structured

³In fact, this generalization applies to any treatments that can be vectorized by feature extraction (pre-defined or learned). We focus on graph treatments as they are a generic representation with many practical applications.

⁴These are also called *meta-learners*. To avoid confusion with *meta-learning*, we call these *plug-in estimators*.

treatments would not only be computationally expensive, but would also not be able to make use of graph features or learn graph representations.

Multiple treatments. While Inverse Probability Weighting (IPW) [32, 33, 67] is a popular technique for estimating effects with multiple, categorical treatments, it requires estimating the propensity density which is infeasible in settings with hundreds or thousands of graph treatments; some of which may have not been seen during training. Nabi et al. [40] propose a framework for sufficient dimensionality reduction of high-dimensional treatments based on semiparametric inference theory. Besides relying on IPW, this approach is designed for average treatment effects (not CATEs).

3 Preliminaries

3.1 Conditional Average Treatment Effects (CATEs)

Imagine a dataset where each example $(\mathbf{x}_i, \mathbf{t}_i, y_i) \in \mathcal{D}$ represents a hospital patient's medical history record \mathbf{x}_i , prescribed drug treatment \mathbf{t}_i , and health outcome y_i , as illustrated in Figure 1 (Center). Further, we wish to understand how changing the treatment changes a patient's health outcome. The CATE, $\tau(\mathbf{t}', \mathbf{t}_i, \mathbf{x}_i)$, describes the expected change in outcome for individuals with history \mathbf{x}_i , when treatment \mathbf{t}_i is replaced by \mathbf{t}' , depicted in Figure 1 (Right). In real-world scenarios, we only observe one outcome for each patient at one treatment level. Further, the patient's pre-treatment health conditions \mathbf{x}_i influence both the doctor's treatment prescription and outcome, thereby *confounding* the effect of the treatment on the outcome.

Formally, we have the dataset $\mathcal{D} = \{(\mathbf{x}_i, \mathbf{t}_i, y_i)\}_{i=1}^n$ sampled from a joint distribution $p(\mathbf{X}, \mathbf{T}, Y)$, where $Y = f(\mathbf{X}, \mathbf{T}) + \varepsilon$, as depicted in Figure 1 (Left). We define the causal effect of fixing *treatment* variable $\mathbf{T} \in \mathcal{T}$ to a value \mathbf{t} on *outcome* variable $Y \in \mathbb{R}$ using the do-operator [44] as $\mathbb{E}[Y \mid \text{do}(\mathbf{T} = \mathbf{t})]$. Crucially, this estimate differs from the conditional expectation $\mathbb{E}[Y \mid \mathbf{T} = \mathbf{t}]$ in that it describes the effect of an external entity *intervening* on \mathbf{T} by fixing it to a value \mathbf{t} . We further condition on pre-treatment *covariates* \mathbf{X} to define the conditional causal estimand $\mathbb{E}[Y \mid \mathbf{X} = \mathbf{x}, \text{do}(\mathbf{T} = \mathbf{t})]$. The *conditional average treatment effect* (CATE) is the difference between expected outcomes at different treatment values \mathbf{t}, \mathbf{t}' for given covariates \mathbf{x} ,

$$\tau(\mathbf{t}', \mathbf{t}, \mathbf{x}) \triangleq \underbrace{\mathbb{E}[Y \mid \mathbf{X} = \mathbf{x}, \text{do}(\mathbf{T} = \mathbf{t}')] - \mathbb{E}[Y \mid \mathbf{X} = \mathbf{x}, \text{do}(\mathbf{T} = \mathbf{t})]}_{=: \mu_{\mathbf{t}'}(\mathbf{x}) - \mu_{\mathbf{t}}(\mathbf{x})}, \quad (1)$$

where $\mu_{\mathbf{t}}(\mathbf{x})$ is defined as the *expected outcome* for a covariate vector \mathbf{x} under treatment \mathbf{t} .

Because we do not observe both treatments \mathbf{t}, \mathbf{t}' for a single covariate \mathbf{x} , we need to make assumptions that allow us to identify the CATE from observational data.

Assumption 1. (*Unconfoundedness*) *There are no confounders of the effect between \mathbf{T} and Y beyond \mathbf{X} . Therefore, $\Pr(Y \leq y \mid \mathbf{x}, \text{do}(\mathbf{t})) = \Pr(Y \leq y \mid \mathbf{x}, \mathbf{t})$, for all $(\mathbf{x}, \mathbf{t}, y)$.*

Assumption 2. (*Overlap*) *It holds that $0 < p(\mathbf{t} \mid \mathbf{x}) < 1$, for all $(\mathbf{x}, \mathbf{t}, y)$.*

Assumption 2 means that all sub-populations have some probability of receiving any value of treatment (otherwise, some $\tau(\mathbf{t}', \mathbf{t}, \mathbf{x})$ may be undefined or impossible to estimate.) These assumptions allow us to estimate the causal quantity $\tau(\mathbf{t}', \mathbf{t}, \mathbf{x})$ through statistical estimands:

$$\tau(\mathbf{t}', \mathbf{t}, \mathbf{x}) = \mu_{\mathbf{t}'}(\mathbf{x}) - \mu_{\mathbf{t}}(\mathbf{x}) = \mathbb{E}[Y \mid \mathbf{X} = \mathbf{x}, \mathbf{T} = \mathbf{t}'] - \mathbb{E}[Y \mid \mathbf{X} = \mathbf{x}, \mathbf{T} = \mathbf{t}]. \quad (2)$$

While one can model $\mu_{\mathbf{t}}(\mathbf{x})$ with regression models, such approaches suffer from *regularization bias* [10, 28, 31] due to two factors: (i) associations between \mathbf{X} and \mathbf{T} , which are to be expected under confounding, and (ii) regularizing for predictive performance instead of effect estimation. Mitigating such biases usually works by transforming the representation of \mathbf{X} and \mathbf{T} to a (regularized) regression problem that will still provide the causal effect, e.g., by using nuisance components.

3.2 Robinson Decomposition

The *Robinson decomposition* [47] is a mathematical expression which allows one to construct a learnable objective of the CATE in binary treatment settings. The *R-learner* [43] is a plug-in estimator

that exploits this expression. Its modeling flexibility, combined with the avoidance of regularization bias, makes it a compelling estimator.

Let the treatment variable be $T \in \{0, 1\}$ and the outcome model $p(y | \mathbf{x}, \mathbf{t})$ parameterized as

$$Y = f(\mathbf{X}, T) + \varepsilon \triangleq \mu_0(\mathbf{X}) + T \times \tau_b(\mathbf{X}) + \varepsilon, \quad (3)$$

where we define error term ε such that $\mathbb{E}[\varepsilon | \mathbf{x}, \mathbf{t}] = \mathbb{E}[\varepsilon | \mathbf{x}] = 0$, and $\tau_b(\mathbf{x}) \triangleq \tau(1, 0, \mathbf{x})$.

Define the *propensity score* $e(\mathbf{x}) \triangleq p(T = 1 | \mathbf{x})$ and the *conditional mean outcome* as

$$m(\mathbf{x}) \triangleq \mathbb{E}[Y | \mathbf{x}] = \mu_0(\mathbf{x}) + e(\mathbf{x}) \tau_b(\mathbf{x}). \quad (4)$$

From model (3) and the previous definitions, it follows that

$$Y - m(\mathbf{X}) = (T - e(\mathbf{X})) \tau_b(\mathbf{X}) + \varepsilon, \quad (5)$$

allowing us to define the estimator

$$\hat{\tau}_b(\cdot) = \arg \min_{\tau_b} \left\{ \frac{1}{n} \sum_{i=1}^n \left(\tilde{y}_i - \tilde{t}_i \times \tau_b(\mathbf{x}_i) \right)^2 + \Lambda(\tau_b(\cdot)) \right\}, \quad (6)$$

where $\tilde{y}_i \triangleq y_i - \hat{m}(\mathbf{x}_i)$ and $\tilde{t}_i \triangleq t_i - \hat{e}(\mathbf{x}_i)$ are pseudo-data points defined through estimated nuisance functions $\hat{m}(\cdot), \hat{e}(\cdot)$, which can be learned separately with any supervised learning algorithm.

3.3 Graph Neural Networks

We consider interventions with relational structures represented by graphs, such as molecules consisting of atoms (nodes) joined by chemical bonds (edges). Special cases include images and sentences (graphs with grid-structure), as well as real-valued vectors (graphs with independent nodes) [8]. Here, a graph $\mathcal{G} := (\mathcal{V}, \mathcal{E})$ consists of a set of vertices $v^{(i)} \in \mathcal{V}$, labeled with vectors $\mathbf{v}^{(i)} \in \mathbb{R}^{m_v}$ and a set of directed edges $e^{ij} \in \mathcal{E}$ from vertex $v^{(i)}$ to $v^{(j)}$, labeled with vectors $\mathbf{e}^{ij} \in \mathbb{R}^{m_e}$. To enable our estimator to operate over graph-structured data, we resort to graph neural networks (GNNs), whose parameters, like those of other neural networks, can be learned through backpropagation.

4 Graph Intervention Networks

Our goal is to estimate the CATE $\tau(\mathbf{t}', \mathbf{t}, \mathbf{x})$ for graph interventions $\mathbf{t} \triangleq \mathcal{G}, \mathbf{t}' \triangleq \mathcal{G}'$. A good estimator should correct for the confounding of \mathbf{X} on \mathbf{T} and Y in the data. For this we appeal to the Robinson decomposition, which has inspired flexible CATE estimation for binary treatments [6, 10, 35, 43].

4.1 Generalizing the Robinson Decomposition

A generic way to extend the Robinson decomposition to arbitrary treatments is to learn a model $\hat{f}(\mathbf{X}, \mathbf{T})$ defined over the entire outcome surface, via mean outcome $\hat{m}(\mathbf{X})$ and treatment conditional density $p(\mathbf{T} | \mathbf{X})$. In this case, we fit the relationship

$$Y - m(\mathbf{X}) = f(\mathbf{X}, \mathbf{T}) - e^p(\mathbf{X}) + \varepsilon, \quad \text{where } e^p(\mathbf{x}) \triangleq \mathbb{E}[f(\mathbf{X}, \mathbf{T}) | \mathbf{x}]. \quad (7)$$

To learn $f(\cdot, \cdot)$ from a dataset $\mathcal{D} = \{(\mathbf{x}_i, \mathbf{t}_i, y_i)\}_{i=1}^n$ we need to solve,

$$\hat{f} = \arg \min_{f \in \mathcal{F}} \frac{1}{N} \sum_{i=1}^N \left[\{y_i - \hat{m}(\mathbf{x}_i)\} - (f(\mathbf{x}_i, \mathbf{t}_i) - \hat{e}^p(\mathbf{x}_i)) \right]^2, \quad (8)$$

where \mathcal{F} is some function space and \hat{m} is a plug-in finite sample estimate of m . Because e^p contains f , we need to estimate it, which we denote \hat{e}^p . One solution is to estimate the propensity $p(\mathbf{T} | \mathbf{X})$ and use it to compute \hat{e}^p . However, this approach requires conditional density estimation over high-dimensional graphs, which remains an open research question [66], and is prone to high variance [58]. Further, to compute \hat{e}^p from it, one has to resort to Monte Carlo evaluation. Another option is to solve for f , fix it, then estimate \hat{e}^p using regression from finite samples, and iterate to a fixed point.

However, there is a fundamental issue with this approach: we are typically interested in regularizing the causal effect directly as opposed to the generic regression function. This is why, for instance, the R-learner parameterizes $\mu_1(\mathbf{x})$ as a (nuisance) baseline $\mu_0(\mathbf{x})$ plus the CATE $\tau_b(\mathbf{x})$. The black-box $f(\mathbf{x}, \mathbf{t})$ does not capture the asymmetry between \mathbf{x} and \mathbf{t} in the implied CATE $f(\mathbf{x}, \mathbf{t}) - f(\mathbf{x}, \mathbf{t}')$. Further, unlike the binary case, in many applications, we do not have a baseline treatment \mathbf{t}_0 with respect to which we could parameterize f in terms of some $\tau(\mathbf{t}, \mathbf{t}_0, \mathbf{x})$.

To address these issues, we take a different route that (a) avoids conditional density estimation over high-dimensional spaces and, (b) partials-out the dependence of \mathbf{X} on \mathbf{T} on Y . For (a), we propose to learn *propensity features*, which, as we will see, have a natural connection to the propensity score, but make inference easier. For (b), we make the assumption that the causal effect of interest is a *product effect*: the outcome function $f(\mathbf{X}, \mathbf{T})$ can be written as an inner product of two high-dimensional functions depending on the covariates and the treatment, respectively. We consider this to be a mild assumption, as we can formally justify its universality.

Assumption 3. (*Product effect*) *We consider the following partial parameterization of $p(y | \mathbf{x}, \mathbf{t})$,*

$$Y = \underbrace{g(\mathbf{X})^\top h(\mathbf{T})}_{=:f(\mathbf{X}, \mathbf{T})} + \varepsilon, \quad (9)$$

where $g : \mathcal{X} \rightarrow \mathbb{R}^d$, $h : \mathcal{T} \rightarrow \mathbb{R}^d$ and $\mathbb{E}[\varepsilon | \mathbf{x}, \mathbf{t}] = \mathbb{E}[\varepsilon | \mathbf{x}] = 0$, for all $(\mathbf{x}, \mathbf{t}) \in \mathcal{X} \times \mathcal{T}$.

The CATE follows as

$$\tau(\mathbf{t}', \mathbf{t}, \mathbf{x}) = g(\mathbf{x})^\top (h(\mathbf{t}') - h(\mathbf{t})). \quad (10)$$

The following asserts that provided we allow the dimensionality of g and h to grow, we may approximate any arbitrary bounded continuous functions in $\mathcal{C}(\mathcal{X} \times \mathcal{T})$ where $\mathcal{X} \times \mathcal{T}$ is compact.

Proposition 1. (*Universality of product effect*) *Let $\mathcal{H}_{\mathcal{X} \times \mathcal{T}}$ be a Reproducing Kernel Hilbert Space (RKHS) on the set $\mathcal{X} \times \mathcal{T}$ with universal kernel k . Under any finite sample regime with N samples, any minimizer of the objective function in eq. (8) where $\mathcal{F} = \mathcal{H}_{\mathcal{X} \times \mathcal{T}}$ can be written as the inner product of two vector fields $g \in (\mathcal{H}_{\mathcal{X}})^d$, $h \in (\mathcal{H}_{\mathcal{T}})^d$ with $d \leq N^2$, where \hat{m} and \hat{e}^p are finite-sample, kernel-ridge-regression estimates of $\mathbb{E}[Y | \mathbf{X}]$ and $\mathbb{E}[f(\mathbf{X}, \mathbf{T}) | \mathbf{X}]$ respectively.*

We defer the proof to Appendix A.1.

4.2 The Robinson Decomposition for Product Effects

Define *propensity features* $e^h(\mathbf{x}) \triangleq \mathbb{E}[h(\mathbf{T}) | \mathbf{x}]$ and $m(\mathbf{x}) \triangleq \mathbb{E}[Y | \mathbf{x}] = g(\mathbf{x})^\top e^h(\mathbf{x})$.

Following the same steps as in Section 3.2, the generalized Robinson decomposition for eq. (9) is

$$Y - m(\mathbf{X}) = g(\mathbf{X})^\top (h(\mathbf{T}) - e^h(\mathbf{X})) + \varepsilon. \quad (11)$$

For a fixed $h(\cdot)$, a direct generalization of the R-learner to graph treatments is the solution of

$$\hat{g}(\cdot) = \arg \min_g \left\{ \frac{1}{n} \sum_{i=1}^n \left(Y_i - \hat{m}(\mathbf{X}_i) - g(\mathbf{X}_i)^\top (h(\mathbf{T}_i) - \hat{e}^h(\mathbf{X}_i)) \right)^2 + \Lambda(g(\cdot)) \right\}. \quad (12)$$

Instead of fixing $h(\cdot)$, we propose to simultaneously learn $h(\cdot)$ using an alternating approach. This allows us to learn representations for both covariates \mathbf{X} and treatments \mathbf{T} that can adapt to each other. This poses the following challenge: learning $\hat{e}^h(\cdot)$ is now entangled with learning $h(\cdot)$. While the R-learner is based on the idea of *cross-fitting*, where at each data point i we pick estimates of the nuisances that do not use that data point⁵, in what follows we introduce a pragmatic representation

⁵For instance, $\hat{m}(\cdot)$ can vary from data point to data point, which can be denoted as $\hat{m}_i(\cdot)$. Under cross-fitting, the requirement is that \hat{m}_i is not a function of $(\mathbf{X}_i, \mathbf{T}_i, Y_i)$.

learning approach for (\hat{g}, \hat{h}) that does not use cross-fitting⁶ while still being able to beat competitor methods in our experimental evaluation. We call this approach *Graph Intervention Networks* (GIN).

4.3 Algorithm

We introduce a two-stage algorithm for training. To allow for both flexibility in representation learning of complex causal relationships as well as scalability to large and high-dimensional data-sets, we instantiate our method using neural networks. In principle however, any model trainable via gradient descent can be used. We learn surrogate models for the mean outcome and propensity features $\hat{m}_\theta(\mathbf{X})$ and $\hat{e}_\eta^h(\mathbf{X})$ with parameters $\theta \in \mathbb{R}^{d_\theta}$, $\eta \in \mathbb{R}^{d_\eta}$, as well as feature maps for covariates and treatments $\hat{g}_\psi(\mathbf{X})$, $\hat{h}_\phi(\mathbf{T})$, parameterized by $\psi \in \mathbb{R}^{d_\psi}$, $\phi \in \mathbb{R}^{d_\phi}$. We denote regularizers by $\Lambda(\cdot)$. Figure 2 summarizes the algorithm. As the mean outcome model $\hat{m}_\theta(\mathbf{X})$ does not depend on the other components, we learn it separately in Stage 1. In Stage 2, we alternate between learning ψ, ϕ, η .

Stage 1: Learn parameters θ of the mean outcome model $\hat{m}_\theta(\mathbf{X})$ based on the objective

$$J_m(\theta) = \sum_{i=1}^m \|y_i - \hat{m}_\theta(\mathbf{x}_i)\|_2^2 + \Lambda(\theta), \quad (13)$$

which relies only on covariates and outcome data $\mathcal{D}_1 := \{(\mathbf{x}_i, y_i)\}_{i=1}^m$.

Stage 2: Learn parameters ψ, ϕ for the covariates and treatments feature maps $\hat{g}_\psi(\mathbf{X})$, $\hat{h}_\phi(\mathbf{T})$, as well as parameters η for the propensity features $\hat{e}_\eta^h(\mathbf{X})$.

$$J_{g,h}(\phi, \psi) = \sum_{i=1}^n \left\| y_i - \left\{ \hat{m}_\theta(\mathbf{x}_i) + \hat{g}_\psi(\mathbf{x}_i)^\top (\hat{h}_\phi(\mathbf{t}_i) - \hat{e}_\eta^h(\mathbf{x}_i)) \right\} \right\|_2^2 + \Lambda(\psi) + \Lambda(\phi). \quad (14)$$

This loss hinges on $\hat{e}_\eta^h(\mathbf{X})$, which needs to be learned by

$$J_{e^h}(\eta) = \sum_{i=1}^n \left\| \hat{h}_\phi(\mathbf{t}_i) - \hat{e}_\eta^h(\mathbf{x}_i) \right\|_2^2 + \Lambda(\eta), \quad (15)$$

and in turn depends on $\hat{h}_\phi(\mathbf{T})$. While it may be tempting to learn ψ, ϕ and η jointly, they have fundamentally different objectives ($\hat{e}_\eta^h(\mathbf{X})$ is defined as an estimate of the expectation $\mathbb{E}[h(\mathbf{T}) | \mathbf{x}]$). Therefore, we employ an alternating optimization procedure, where we take $k \in \{1, \dots, K\}$ optimization steps for ψ, ϕ towards $J_{g,h}(\psi, \phi)$ and one step for learning η . We observe that setting $K > 1$, i.e. updating ψ, ϕ more frequently than η , stabilizes the training process.

4.4 Advantages of GINs

We conclude by describing the beneficial properties of GIN, particularly in finite-sample regimes:

1. **Targeted regularization:** Regularizing $\hat{g}_\psi(\mathbf{X}), \hat{h}_\phi(\mathbf{T})$ in eq. (14) after partialing out confounding allows for a type of targeted regularization of the isolated causal effect. We will show that this leads to improved estimation. In contrast, outcome estimation methods can suffer from regularization-induced confounding, i.e., inadvertently regularizing the causal effect estimate away from zero in the service of trying to improve predictive performance [9, 11, 17, 28, 31, 43].
2. **Propensity features:** There are often parts of \mathbf{X} that cause the treatment but not the outcome; to avoid modeling them is one of the attractions of regression-based causal inference [21]. Likewise, we would like to dispose of unnecessary components of a high-dimensional \mathbf{T} , but there is little in the literature about what to do when a criterion such as Robinson decomposition is used to define a method. Propensity features are a way to avoid using $p(\mathbf{t} | \mathbf{x})$ as a nuisance parameter.

⁶We could in principle use cross-fitting for \hat{e}^h , although the loop between fitting \hat{h} alternating with \hat{e}^h would break the overall independence between $\hat{e}_i^h(\cdot)$ and data point i . While it is possible that cross-fitting for \hat{e}^h is still beneficial in this case, for simplicity and for computational savings, we did not implement it.

a GIN Training.

Input: Stage 1 data $\mathcal{D}_1 := \{(\mathbf{x}_i, y_i)\}_{i=1}^m$, Stage 2 data $\mathcal{D}_2 := \{(\mathbf{x}_i, \mathbf{t}_i, y_i)\}_{i=1}^n$ Step sizes $\lambda_\theta, \lambda_\eta, \lambda_\psi, \lambda_\phi$. Number of update steps K . Mini-batch sizes B_1, B_2 .

```
1: Initialize parameters:  $\theta, \eta, \psi, \phi$ 
2: while not converged do            $\triangleright$  Stage 1
3:   Sample mini-batch  $\{(\mathbf{x}_b, y_b)\}_{b=1}^{m_{B_1}}$ 
4:   Evaluate  $J_m(\theta)$ 
5:   Update  $\theta \leftarrow \theta - \lambda_\theta \hat{\nabla}_\theta J(\theta)$ 
6: end while
7: while not converged do            $\triangleright$  Stage 2
8:   Sample mini-batch  $\{(\mathbf{x}_b, \mathbf{t}_b, y_b)\}_{b=1}^{m_{B_2}}$ 
9:   Evaluate  $J_{g,h}(\psi, \phi), J_{e^h}(\eta)$ 
10:  for  $k = 1$  to  $K$  do
11:    Update  $\phi \leftarrow \phi - \lambda_\phi \hat{\nabla}_\phi J_{g,h}(\psi, \phi)$ 
12:    Update  $\psi \leftarrow \psi - \lambda_\psi \hat{\nabla}_\psi J_{g,h}(\psi, \phi)$ 
13:  end for
14:  Update  $\eta \leftarrow \eta - \lambda_\eta \hat{\nabla}_\eta J_{e^h}(\eta)$ 
15: end while
```

b Pseudocode in a PyTorch-like style.

```
# Initialize submodels and optimizers
m, e, g, h = MLP(...), MLP(...), MLP(...),
             GNN(...)
m_opt, e_opt, g_opt, h_opt = Adam(m.params(), ...,
                                   m_lr), Adam(e.params(), e_lr), ...
```

```
# Stage 1
for batch in train_loader:
    X, Y = batch.X, batch.Y
    m_opt.zero_grad()
    F.mse_loss(m(X), Y).backward()
    m_opt.step()
```

```
# Stage 2
for batch in train_loader:
    X, T, Y = batch.X, batch.T, batch.Y
    for _ in range(num_update_steps):
        g_opt.zero_grad()
        h_opt.zero_grad()
        F.mse_loss((g(X)*(h(T) - e(X))).sum
                   (-1), (Y-m(X))).backward()
        g_opt.step()
        h_opt.step()
        e_opt.zero_grad()
        F.mse_loss(e(X), h(T)).backward()
        e_opt.step()
```

Figure 2: The two-stage algorithm for training GIN.

3. **Data-efficiency:** In contrast to methods that split the data into disjoint models for each treatment group (known as *T-learners* for binary treatments [9, 11]), sharing causal effect parameters between all covariates regardless of their assigned treatment increases data-efficiency, especially if certain graph interventions are only observed a few times and are supported on few covariates.
4. **Partial data:** In settings without access to both the treatment assignment and the outcome but only access to one of them, one can leverage that data to improve our estimator further. A typical scenario is significant lags between applying a treatment and observing the outcome, e.g., a patients’ recovery in one year after a drug was administered [35]. There is data about the treatment in such scenarios that may refine the estimate of $\hat{e}_\eta^h(\mathbf{X})$. Analogously, if only treatment data is missing, one can use covariates and outcome data to improve $\hat{m}_\theta(\mathbf{X})$.

5 Experiments

The goal of our experiments is to understand how deconfounding through the generalized Robinson decomposition compares with prior methods in graph intervention settings.

5.1 Experimental Setup

Datasets. To be able to compute CATE estimation error w.r.t. a ground truth, we design two causal models: a simpler synthetic model with small-world graph treatments and a more complex model with real-world molecular graph treatments and gene expression covariates. The Small-World (SW) simulation contains 1,000 uniformly sampled covariates and 200 randomly generated Watts–Strogatz small-world graphs [62] as treatments. *The Cancer Genomic Atlas* (TCGA) simulation uses 9,659 gene expression measurements of cancer patients for covariates [63] and 10,000 sampled molecules from the QM9 dataset [46] as treatments. Appendix C details the data-generating schemes.

Baselines. We compare our method to (1) **Zero**, a sanity-check baseline that consistently predicts zero treatment effect and equals the mean squared treatment effect (poorly regularized models may perform worse than that due to confounding), (2) **CAT**, a categorical treatment variable model using one-hot encoded treatment indicator vectors, (3) **GNN**, a model that first encodes treatments with a GNN and then concatenates treatment and individual features for regression, (4) **GraphITE** [18], a CATE estimation method designed for graph treatments (more details in Section 2). GNN and CAT reflect the performance of standard regression models. The contrast between these two provides

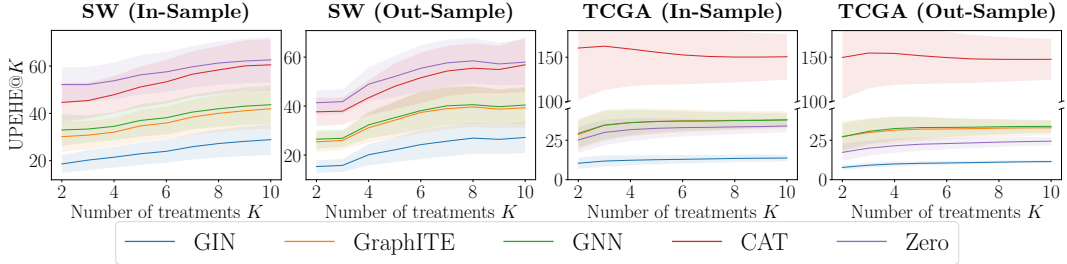


Figure 3: UPEHE@ K for $K \in \{2, \dots, 10\}$.

Table 1: Error of CATE estimation for all methods, measured by WPEHE@6. Results are averaged over 10 trials, \pm denotes std. error (each trial samples treatment assignment matrix \mathbf{W}).

Method	SW		TCGA	
	In-sample	Out-sample	In-sample	Out-sample
Zero	56.26 ± 8.12	53.77 ± 8.93	26.63 ± 7.55	17.94 ± 4.86
CAT	51.75 ± 8.85	49.76 ± 9.73	155.88 ± 52.82	146.62 ± 42.32
GNN	37.10 ± 6.84	36.74 ± 7.42	30.67 ± 8.29	27.57 ± 7.95
GraphITE	34.81 ± 6.70	35.94 ± 8.07	30.31 ± 8.96	27.48 ± 8.95
GIN	23.00 ± 4.56	23.19 ± 5.56	10.98 ± 3.45	8.15 ± 1.46

insight into whether the additional graph structure of the treatment improves CATE estimation. To deal with unseen treatments during CAT’s evaluation, we map such to the most similar ones seen during training based on their Euclidean distance in the embedding space of the GNN baseline.

Graph models. For small-world networks, we use *k-dimensional GNNs* [39], as to distinguish graphs they take higher-order structures into account. To model molecular graphs, we use *Relational Graph Convolutional Networks* [50], where the nodes are atoms and each edge type corresponds to a specific bond type. We use the implementations of PyTorch Geometric [12].

Evaluation metrics. We extend the *expected Precision in Estimation of Heterogeneous Effect* (PEHE) commonly used in binary treatment settings [21] to arbitrary pairs of treatments $(\mathbf{t}, \mathbf{t}')$ as follows. We denote the *Unweighted PEHE* (UPEHE) and the *Weighted PEHE* (WPEHE) as

$$\epsilon_{\text{UPEHE}(\text{WPEHE})} \triangleq \int_{\mathcal{X}} \left(\hat{\tau}(\mathbf{t}', \mathbf{t}, \mathbf{x}) - \tau(\mathbf{t}', \mathbf{t}, \mathbf{x}) \right)^2 p(\mathbf{t} | \mathbf{x}) p(\mathbf{t}' | \mathbf{x}) p(\mathbf{x}) d\mathbf{x}, \quad (16)$$

where the weighted version gives less importance to treatment pairs that are less likely; to account for the fact that such pairs will have higher estimation errors. In fact, as the reliability of estimated effects decreases by how likely they are in the observational study, we evaluate all methods on U/WPEHE truncated to the top K treatments, which we call U/WPEHE@ K . To compute this, for each \mathbf{x} , we rank all treatments by their propensity $p(\mathbf{t} | \mathbf{x})$ (given by the causal model) in descending order. We take the top K treatments and compute the U/WPEHE for all $\binom{K}{2}$ treatment pairs.

In-sample vs. out-sample. A common benchmark for causal inference methods is the *in-sample* task, which we include here for completeness: estimating CATEs for covariate values \mathbf{x} found in the training set. This task is still non-trivial, as the outcome of only one treatment is observed during training⁷. In contrast, and arguably of more relevance to decision making, the goal of the *out-sample* task is to estimate CATEs for completely unseen covariate realizations \mathbf{x}' .

Hyper-parameter tuning. To ensure a fair comparison, we perform hyper-parameter optimization with random search for all models on held-out data and select the best hyper-parameters over 10 runs.

Propensity. We define the propensity (or *treatment selection bias*) as $p(\mathbf{T} | \mathbf{x}) = \text{softmax}(\kappa \mathbf{W}^\top \mathbf{X})$, where $\mathbf{W} \in \mathbb{R}^{|\mathcal{T}| \times d}$, $\forall i, j : W_{ij} \sim \mathcal{U}[0, 1]$ is a random matrix (sampled

⁷The original motivation comes from Fisherian designs where the only source of randomness is on the treatment assignment [22]. Our motivation is simpler: rule out the extra variability from different covariates, highlighting the difference between methods due to different loss functions and less due to smoothing abilities.

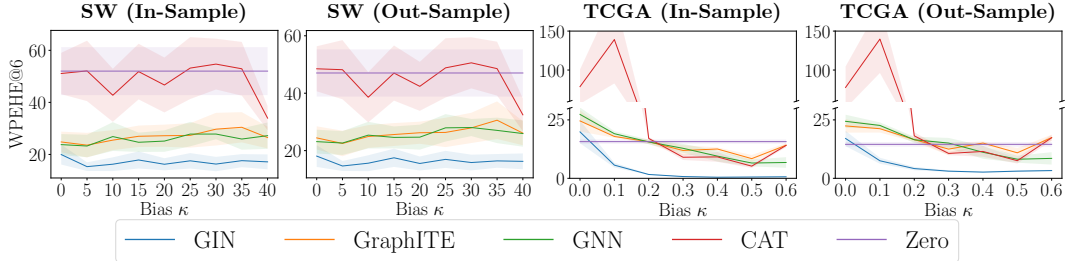


Figure 4: WPEHE@6 over increasing bias strength κ .

then fixed for each run). Recall $|\mathcal{T}|$ is the number of available treatments and let d be the dimensionality of the covariates. Here the *bias strength* κ is a temperature parameter that determines the flatness of the propensity (the lower the flatter, i.e., $\kappa=0$ corresponds to the uniform distribution).

5.2 Comparison of Performances on different K Treatments

Figure 3 shows the UPEHE@ K of all methods for $K \in \{2, \dots, 10\}$. We also report the WPEHE@6 of all methods in Table 1. Unless stated otherwise, we report results for bias strengths $\kappa = 10$ and $\kappa = 0.1$ in the SW and TCGA datasets, respectively across 10 random trials.

The results indicate that the relative performance of each method, for both the in-sample and out-sample estimation tasks, is consistent. Further, they suggest that, overall, the performance of GIN is best due to a better isolation of the causal effect from the observed data compared to other methods. The performance difference between CAT and GNN across all results indicate that accounting for graph information significantly improves the estimates. We observe from the SW experiments that GraphITE [18] performs slightly better than GNN, while it is nearly the same as GNN on TCGA.

Surprisingly, the results of the TCGA experiments with low bias strength $\kappa = 0.1$ expose that all models but GIN fail to isolate causal effects better than the Zero baseline. These results confirm that confounding effects of \mathbf{X} on \mathbf{Y} combined with moderate causal effects can cause severe regularization bias for black-box regression models, while GIN partials these out from the outcome by $\hat{m}_\theta(\mathbf{X})$. We include additional results on convergence and larger values of K in the Appendix.

5.3 Comparison of Robustness to different Bias Strengths κ

A strong selection bias (i.e. large κ) in the observed data makes CATE estimation more difficult, as it becomes unlikely to see certain treatments $\mathbf{t} \in \mathcal{T}$ for particular covariates \mathbf{x} . Here, we assess each model’s robustness to varying levels of selection bias, determined by κ , across 5 random seeds. In Figure 4, we see that GIN outperforms the baselines across the entire range of considered biases. Interestingly, GIN performs competitively even in a case with no selection bias ($\kappa = 0$, which corresponds to a randomized experiment). Importantly, all performances seem to either stagnate (SW) or to increase (TCGA) with increasing biases. Notably, the poor performance of CAT suddenly improves on datasets with high bias. We believe this is because, in high bias regimes, we see fewer distinct treatments overall, which allows the CAT model to approach the performance of GNN.

6 Limitations, Future Work and Potential Negative Societal Impacts

Limitations and future work. One limitation of the current work is the lack of a convergence guarantee for estimating $\hat{g}_\psi(\mathbf{X})$, $\hat{h}_\phi(\mathbf{T})$, as is done in the R-Learner [43]. Our first direction of future work is thus adapting the quasi-oracle guarantee of Nie & Wager [43] to this setting. This guarantee would help to theoretically characterize the extent to which our objective mitigates regularization bias present in traditional regression methods. Second, in some real-life domains, Assumption 1 (Unconfoundedness) can be too strong, as there may exist *hidden confounders*. There are two common strategies to deal with them: utilizing *instrumental variables* [19, 58, 64] or *proxy variables* [37, 38, 59]. Developing new approaches for graph interventions in such settings is a promising future direction. Finally, neural network initialization can impact final estimates. To obtain consistency guarantees, kernel methods can be used [37, 58]. Investigating a kernel formulation of our objective is thus an interesting direction for future work.

Potential negative societal impacts. Because causal inference methods make recommendations about interventions to apply in real-world settings, misapplying them can have a negative real-world impact. This issue applies to all research in causal effect estimation. It is crucial to thoroughly test these methods on realistic simulations and alter aspects of them to understand how violations of assumptions impact estimation. There is a significant sub-field of causal inference devoted to such sensitivity analyses. We have aimed to provide a comprehensive evaluation of graph treatment methods by showing how estimation degrades as less likely treatments are considered (Figure 3) and as treatment bias increases (Figure 4). When applying this method in practice, there are additional sensitivity analysis tools that should be leveraged [15, 60] to mitigate negative impacts.

7 Conclusion

This paper introduced GIN, a method for CATE estimation with graph interventions. GIN generalizes the Robinson decomposition to isolate the causal estimand from confounding associations. Our plug-in estimator supports any supervised learning method. In experiments, GIN outperforms baseline CATE estimators for graph treatments, across multiple treatment pairs and bias levels.

Acknowledgements

We thank Antonin Schrab, David Watson, Jakob Zeitler, Limor Gultchin, Marc Deisenroth and Shonosuke Harada for useful discussions and constructive feedback on the paper. JK and YZ acknowledge support by the Engineering and Physical Sciences Research Council with grant number EP/S021566/1. This work was partially supported by an ONR grant number N62909-19-1-2096 to RS. We acknowledge the generous provision of Azure cloud computing resources by the Alan Turing Institute.

References

- [1] Alaa, A. and van der Schaar, M. Limits of estimating heterogeneous treatment effects: Guidelines for practical algorithm design. In Dy, J. and Krause, A. (eds.), *Proceedings of the 35th International Conference on Machine Learning*, volume 80 of *Proceedings of Machine Learning Research*, pp. 129–138, Stockholm, Sweden, 10–15 Jul 2018. PMLR.
- [2] Alaa, A. M. and van der Schaar, M. Bayesian inference of individualized treatment effects using multi-task gaussian processes. In Guyon, I., Luxburg, U. V., Bengio, S., Wallach, H., Fergus, R., Vishwanathan, S., and Garnett, R. (eds.), *Advances in Neural Information Processing Systems*, volume 30. Curran Associates, Inc., 2017.
- [3] Arbour, D., Dimmery, D., and Sondhi, A. Permutation weighting. *arXiv preprint arXiv:1901.01230*, 2020.
- [4] Athey, S. and Imbens, G. Recursive partitioning for heterogeneous causal effects. *Proceedings of the National Academy of Sciences*, 113(27):7353–7360, 2016.
- [5] Athey, S. and Wager, S. Estimating treatment effects with causal forests: An application. *arXiv preprint arXiv:1902.07409*, 2019.
- [6] Athey, S., Tibshirani, J., and Wager, S. Generalized random forests. *The Annals of Statistics*, 47(2):1148 – 1178, 2019. doi: 10.1214/18-AOS1709.
- [7] Bica, I., Jordon, J., and van der Schaar, M. Estimating the effects of continuous-valued interventions using generative adversarial networks. In Larochelle, H., Ranzato, M., Hadsell, R., Balcan, M., and Lin, H. (eds.), *Advances in Neural Information Processing Systems 33: Annual Conference on Neural Information Processing Systems 2020, NeurIPS 2020, December 6-12, 2020, virtual*, 2020.
- [8] Bronstein, M. M., Bruna, J., Cohen, T., and Veličković, P. Geometric deep learning: Grids, groups, graphs, geodesics, and gauges. *arXiv preprint arXiv:2104.13478*, 2021.
- [9] Caron, A., Manolopoulou, I., and Baio, G. Estimating individual treatment effects using non-parametric regression models: a review. *arXiv preprint arXiv:2009.06472*, 2020.

[10] Chernozhukov, V., Chetverikov, D., Demirer, M., Duflo, E., Hansen, C., Newey, W., and Robins, J. Double/debiased machine learning for treatment and structural parameters. *The Econometrics Journal*, 21(1):C1–C68, 01 2018. ISSN 1368-4221.

[11] Curth, A. and van der Schaar, M. Nonparametric estimation of heterogeneous treatment effects: From theory to learning algorithms. In Banerjee, A. and Fukumizu, K. (eds.), *The 24th International Conference on Artificial Intelligence and Statistics, AISTATS 2021, April 13-15, 2021, Virtual Event*, volume 130 of *Proceedings of Machine Learning Research*, pp. 1810–1818. PMLR, 2021.

[12] Fey, M. and Lenssen, J. E. Fast graph representation learning with PyTorch Geometric. In *ICLR Workshop on Representation Learning on Graphs and Manifolds*, 2019.

[13] Flaxman, S., Mishra, S., Gandy, A., Unwin, H. J. T., Mellan, T. A., Coupland, H., Whittaker, C., Zhu, H., Berah, T., Eaton, J. W., et al. Estimating the effects of non-pharmaceutical interventions on covid-19 in europe. *Nature*, 584(7820):257–261, 2020.

[14] for Health Statistics, N. C. et al. 2007–2008 national health and nutrition examination survey (nhanes). *US Department of Health and Human Services, Centers for Disease Control and Prevention: Hyattsville, MD, USA*, 2008.

[15] Franks, A., D’Amour, A., and Feller, A. Flexible sensitivity analysis for observational studies without observable implications. *Journal of the American Statistical Association*, 2019.

[16] Gretton, A., Fukumizu, K., Teo, C. H., Song, L., Schölkopf, B., and Smola, A. J. A kernel statistical test of independence. In Platt, J. C., Koller, D., Singer, Y., and Roweis, S. T. (eds.), *Advances in Neural Information Processing Systems 20, Proceedings of the Twenty-First Annual Conference on Neural Information Processing Systems, Vancouver, British Columbia, Canada, December 3-6, 2007*, pp. 585–592. Curran Associates, Inc., 2007.

[17] Hahn, P. R., Murray, J. S., Carvalho, C. M., et al. Bayesian regression tree models for causal inference: Regularization, confounding, and heterogeneous effects (with discussion). *Bayesian Analysis*, 15(3):965–1056, 2020.

[18] Harada, S. and Kashima, H. Graphite: Estimating individual effects of graph-structured treatments. *arXiv preprint arXiv:2009.14061*, 2020.

[19] Hartford, J., Lewis, G., Leyton-Brown, K., and Taddy, M. Deep IV: A flexible approach for counterfactual prediction. In Precup, D. and Teh, Y. W. (eds.), *Proceedings of the 34th International Conference on Machine Learning*, volume 70 of *Proceedings of Machine Learning Research*, pp. 1414–1423. PMLR, 06–11 Aug 2017.

[20] Hatt, T. and Feuerriegel, S. Estimating average treatment effects via orthogonal regularization. *arXiv preprint arXiv:2101.08490*, 2021.

[21] Hill, J. L. Bayesian nonparametric modeling for causal inference. *Journal of Computational and Graphical Statistics*, 20(1):217–240, 2011. doi: 10.1198/jcgs.2010.08162.

[22] Imbens, G. and Rubin, D. *Causal Inference for Statistics, Social, and Biomedical Sciences*. Cambridge University Press, 2015.

[23] Imbens, G. W. Nonparametric estimation of average treatment effects under exogeneity: A review. *The Review of Economics and Statistics*, 86(1):4–29, 2004. doi: 10.1162/003465304323023651.

[24] Jesson, A., Mindermann, S., Shalit, U., and Gal, Y. Identifying causal-effect inference failure with uncertainty-aware models. *Advances in Neural Information Processing Systems*, 33, 2020.

[25] Jesson, A., Mindermann, S., Gal, Y., and Shalit, U. Quantifying ignorance in individual-level causal-effect estimates under hidden confounding. In *International Conference on Machine Learning*. PMLR, 2021.

[26] Johansson, F., Shalit, U., and Sontag, D. Learning representations for counterfactual inference. In *International conference on machine learning*, pp. 3020–3029. PMLR, 2016.

[27] Kallus, N. DeepMatch: Balancing deep covariate representations for causal inference using adversarial training. In III, H. D. and Singh, A. (eds.), *Proceedings of the 37th International Conference on Machine Learning*, volume 119 of *Proceedings of Machine Learning Research*, pp. 5067–5077. PMLR, 13–18 Jul 2020.

[28] Kennedy, E. H. Optimal doubly robust estimation of heterogeneous causal effects. *arXiv preprint arXiv:2004.14497*, 2020.

[29] Kennedy, E. H., Ma, Z., McHugh, M. D., and Small, D. S. Nonparametric methods for doubly robust estimation of continuous treatment effects. *Journal of the Royal Statistical Society. Series B, Statistical Methodology*, 79(4):1229, 2017.

[30] Kingma, D. P. and Ba, J. Adam: A method for stochastic optimization. In Bengio, Y. and LeCun, Y. (eds.), *3rd International Conference on Learning Representations, ICLR 2015, San Diego, CA, USA, May 7-9, 2015, Conference Track Proceedings*, 2015.

[31] Künzel, S. R., Sekhon, J. S., Bickel, P. J., and Yu, B. Metalearners for estimating heterogeneous treatment effects using machine learning. *Proceedings of the National Academy of Sciences*, 116(10):4156–4165, 2019. ISSN 0027-8424. doi: 10.1073/pnas.1804597116.

[32] Li, F. et al. Propensity score weighting for causal inference with multiple treatments. *Annals of Applied Statistics*, 13(4):2389–2415, 2019.

[33] Lopez, M. J. and Gutman, R. Estimation of causal effects with multiple treatments: a review and new ideas. *Statistical Science*, pp. 432–454, 2017.

[34] Louizos, C., Shalit, U., Mooij, J. M., Sontag, D., Zemel, R., and Welling, M. Causal effect inference with deep latent-variable models. In Guyon, I., Luxburg, U. V., Bengio, S., Wallach, H., Fergus, R., Vishwanathan, S., and Garnett, R. (eds.), *Advances in Neural Information Processing Systems*, volume 30. Curran Associates, Inc., 2017.

[35] Lu, D., Tao, C., Chen, J., Li, F., Guo, F., and Carin, L. Reconsidering generative objectives for counterfactual reasoning. In Larochelle, H., Ranzato, M., Hadsell, R., Balcan, M. F., and Lin, H. (eds.), *Advances in Neural Information Processing Systems*, volume 33, pp. 21539–21553. Curran Associates, Inc., 2020.

[36] Ma, K. W., Lewis, J. P., and Kleijn, W. B. The HSIC bottleneck: Deep learning without back-propagation. In *The Thirty-Fourth AAAI Conference on Artificial Intelligence, AAAI 2020, The Thirty-Second Innovative Applications of Artificial Intelligence Conference, IAAI 2020, The Tenth AAAI Symposium on Educational Advances in Artificial Intelligence, EAAI 2020, New York, NY, USA, February 7-12, 2020*, pp. 5085–5092. AAAI Press, 2020.

[37] Mastouri, A., Zhu, Y., Gultchin, L., Korba, A., Silva, R., Kusner, M. J., Gretton, A., and Muandet, K. Proximal causal learning with kernels: Two-stage estimation and moment restriction. In *International Conference on Machine Learning*. PMLR, 2021.

[38] Miao, W., Geng, Z., and Tchetgen, E. T. Identifying causal effects with proxy variables of an unmeasured confounder. *arXiv preprint arXiv:1609.08816*, 2018.

[39] Morris, C., Ritzert, M., Fey, M., Hamilton, W. L., Lenssen, J. E., Rattan, G., and Grohe, M. Weisfeiler and leman go neural: Higher-order graph neural networks. *Proceedings of the AAAI Conference on Artificial Intelligence*, 33(01):4602–4609, Jul. 2019. doi: 10.1609/aaai.v33i02.33014602.

[40] Nabi, R., McNutt, T., and Shpitser, I. Semiparametric causal sufficient dimension reduction of high dimensional treatments. *arXiv preprint arXiv:1710.06727*, 2020.

[41] Neal, B., Huang, C.-W., and Raghupathi, S. Realcause: Realistic causal inference benchmarking. *arXiv preprint arXiv:2011.15007*, 2021.

[42] Nie, L., Ye, M., qiang liu, and Nicolae, D. {VCN}et and functional targeted regularization for learning causal effects of continuous treatments. In *International Conference on Learning Representations*, 2021.

[43] Nie, X. and Wager, S. Quasi-oracle estimation of heterogeneous treatment effects. *Biometrika*, 09 2020. ISSN 0006-3444. doi: 10.1093/biomet/asaa076.

[44] Pearl, J. *Causality: models, reasoning, and inference*. Cambridge University Press, 2000.

[45] Pollmann, M. Causal inference for spatial treatments. *arXiv preprint arXiv:2011.00373*, 2020.

[46] Ramakrishnan, R., Dral, P. O., Rupp, M., and von Lilienfeld, O. A. Quantum chemistry structures and properties of 134 kilo molecules. *Scientific Data*, 1, 2014.

[47] Robinson, P. M. Root-n-consistent semiparametric regression. *Econometrica*, 56(4):931–954, 1988. ISSN 00129682, 14680262.

[48] ROSENBAUM, P. R. and RUBIN, D. B. The central role of the propensity score in observational studies for causal effects. *Biometrika*, 70(1):41–55, 04 1983. ISSN 0006-3444. doi: 10.1093/biomet/70.1.41.

[49] Ruddigkeit, L., van Deursen, R., Blum, L. C., and Reymond, J.-L. Enumeration of 166 billion organic small molecules in the chemical universe database gdb-17. *Journal of Chemical Information and Modeling*, 52(11):2864–2875, 2012. doi: 10.1021/ci300415d. PMID: 23088335.

[50] Schlichtkrull, M. S., Kipf, T. N., Bloem, P., van den Berg, R., Titov, I., and Welling, M. Modeling relational data with graph convolutional networks. In Gangemi, A., Navigli, R., Vidal, M., Hitzler, P., Troncy, R., Hollink, L., Tordai, A., and Alam, M. (eds.), *The Semantic Web - 15th International Conference, ESWC 2018, Heraklion, Crete, Greece, June 3-7, 2018, Proceedings*, volume 10843 of *Lecture Notes in Computer Science*, pp. 593–607. Springer, 2018.

[51] Schwab, P., Linhardt, L., and Karlen, W. Perfect match: A simple method for learning representations for counterfactual inference with neural networks. *arXiv preprint arXiv:1810.00656*, 2019.

[52] Schwab, P., Linhardt, L., Bauer, S., Buhmann, J. M., and Karlen, W. Learning Counterfactual Representations for Estimating Individual Dose-Response Curves. In *AAAI Conference on Artificial Intelligence*, 2020.

[53] Sejdinovic, D. and Gretton, A. What is an rkhs?, 2014. URL http://www.stats.ox.ac.uk/~sejdinov/teaching/atml14/Theory_2014.pdf.

[54] Shalit, U., Johansson, F. D., and Sontag, D. Estimating individual treatment effect: generalization bounds and algorithms. In *International Conference on Machine Learning*, pp. 3076–3085. PMLR, 2017.

[55] Shi, C., Blei, D., and Veitch, V. Adapting neural networks for the estimation of treatment effects. In Wallach, H., Larochelle, H., Beygelzimer, A., d’Alché-Buc, F., Fox, E., and Garnett, R. (eds.), *Advances in Neural Information Processing Systems*, volume 32. Curran Associates, Inc., 2019.

[56] Shi, C., Veitch, V., and Blei, D. Invariant representation learning for treatment effect estimation. *arXiv preprint arXiv:2011.12379*, 2020.

[57] Silva, R. Observational-interventional priors for dose-response learning. In Lee, D., Sugiyama, M., Luxburg, U., Guyon, I., and Garnett, R. (eds.), *Advances in Neural Information Processing Systems*, volume 29. Curran Associates, Inc., 2016.

[58] Singh, R., Sahani, M., and Gretton, A. Kernel instrumental variable regression. In Wallach, H. M., Larochelle, H., Beygelzimer, A., d’Alché-Buc, F., Fox, E. B., and Garnett, R. (eds.), *Advances in Neural Information Processing Systems 32: Annual Conference on Neural Information Processing Systems 2019, NeurIPS 2019, December 8-14, 2019, Vancouver, BC, Canada*, pp. 4595–4607, 2019.

[59] Tchetgen, E. J. T., Ying, A., Cui, Y., Shi, X., and Miao, W. An introduction to proximal causal learning. *arXiv preprint arXiv:2009.10982*, 2020.

[60] VanderWeele, T. J. and Ding, P. Sensitivity analysis in observational research: introducing the e-value. *Annals of internal medicine*, 167(4):268–274, 2017.

[61] Wager, S. and Athey, S. Estimation and inference of heterogeneous treatment effects using random forests. *Journal of the American Statistical Association*, 113(523):1228–1242, 2018.

[62] Watts, D. J. and Strogatz, S. H. Collective dynamics of ‘small-world’ networks. *nature*, 393(6684):440–442, 1998.

[63] Weinstein, J. N., Collisson, E. A., Mills, G. B., Shaw, K. R. M., Ozenberger, B. A., Ellrott, K., Shmulevich, I., Sander, C., and Stuart, J. M. The cancer genome atlas pan-cancer analysis project. *Nature genetics*, 45(10):1113–1120, 2013.

[64] Xu, L., Chen, Y., Srinivasan, S., de Freitas, N., Doucet, A., and Gretton, A. Learning deep features in instrumental variable regression. In *International Conference on Learning Representations*, 2021.

[65] Yao, L., Li, S., Li, Y., Huai, M., Gao, J., and Zhang, A. Representation learning for treatment effect estimation from observational data. In Bengio, S., Wallach, H., Larochelle, H., Grauman, K., Cesa-Bianchi, N., and Garnett, R. (eds.), *Advances in Neural Information Processing Systems*, volume 31. Curran Associates, Inc., 2018.

- [66] Zhang, D. W., Burghouts, G. J., and Snoek, C. G. M. Set prediction without imposing structure as conditional density estimation. In *International Conference on Learning Representations*, 2021.
- [67] Zhou, Z., Athey, S., and Wager, S. Offline multi-action policy learning: Generalization and optimization. *arXiv preprint arXiv:1810.04778*, 2018.
- [68] Zhu, Y., Coffman, D. L., and Ghosh, D. A boosting algorithm for estimating generalized propensity scores with continuous treatments. *Journal of Causal Inference*, 3(1):25–40, 2015. doi: doi:10.1515/jci-2014-0022.

A Proofs

A.1 Universality of Product Decomposition

We demonstrate that $g(\mathbf{X})^\top h(\mathbf{T})$ is a flexible representation of $f(\mathbf{X}, \mathbf{T})$ by first applying the Representer Theorem to obtain a finite-sample-representation of f and then exploiting the product kernel representation yielded by the isometric isomorphism [53] between the corresponding Reproducing Kernel Hilbert Spaces (RKHSs) of functions on $\mathcal{X} \times \mathcal{T}$.

Suppose $f \in \mathcal{H}_{\mathcal{X} \times \mathcal{T}}$ where $\mathcal{H}_{\mathcal{X} \times \mathcal{T}}$ denote the RKHS of functions on $\mathcal{X} \times \mathcal{T}$ with kernel k . It can be shown that $\mathcal{H}_{\mathcal{X} \times \mathcal{T}}$ is isometrically isomorphic to $\mathcal{H}_{\mathcal{X}} \times \mathcal{H}_{\mathcal{T}}$ with kernels $k_{\mathcal{X}}$ and $k_{\mathcal{T}}$ respectively [53], and where $k_{\mathcal{X} \times \mathcal{T}}((\mathbf{x}_1, \mathbf{t}_1), (\mathbf{x}_2, \mathbf{t}_2)) = k_{\mathcal{X}}(\mathbf{x}_1, \mathbf{x}_2) k_{\mathcal{T}}(\mathbf{t}_1, \mathbf{t}_2)$.

Then, we take advantage of the *Representer Theorem*, which states that the empirical minimizer of any such function is a finite sum of kernels centered at the samples.

But first we adapt the Representer Theorem to our setting, since its original formulation does not deal with conditional expectations of the target function. In our extension, we use the empirical loss w.r.t. f induced by the Robinson decomposition in eq. (8). Mastouri et al. [37] provide a similar argument; however, they do not formally state the extension of the Representer Theorem.

To summarize, in the following, we proceed in two steps: (i) establishing the necessary Representer Theorem Extension, and subsequently (ii) proving the universality of the proposed product effect.

Lemma 2 (Representer Theorem Extension). *Consider a positive definite real kernel: $(\mathcal{X} \times \mathcal{T})^2 \rightarrow \mathbb{R}$ on a non-empty set $\mathcal{X} \times \mathcal{T}$ with a corresponding Reproducing Kernel Hilbert Space $\mathcal{H}_{\mathcal{X} \times \mathcal{T}}$. Let there be given*

- a dataset $\{(\mathbf{x}_1, \mathbf{t}_1, \mathbf{y}_1), \dots, (\mathbf{x}_n, \mathbf{t}_n, \mathbf{y}_n)\} \in \mathcal{X} \times \mathcal{T} \times \mathbb{R}$.
- a strictly increasing real-valued function $\Omega: [0, \infty) \rightarrow \mathbb{R}$, and
- an arbitrary error function $E: (\mathcal{X} \times \mathcal{T} \times \mathbb{R}^2)^s \rightarrow \mathbb{R} \cup \{\infty\}$. $s \leq n$.
- a function $\zeta: \mathcal{X} \rightarrow \mathbb{R}$.
- An Kernel Ridge Regression estimator for the kernel conditional mean embedding of $\mathbf{T} | \mathbf{X}$, $\mu(\mathbf{T} | \mathbf{X})$, which we denote as $\hat{\mu}_{KRR}^{\tilde{s}}(\mathbf{T} | \mathbf{X})$. To obtain $\hat{\mu}_{KRR}^{\tilde{s}}(\mathbf{T} | \mathbf{X})$, we use a subsample of the training sample, say $\{(\mathbf{x}_{\rho(j)}, \mathbf{t}_{\rho(j)}, \mathbf{y}_{\rho(j)}): j = 1, \dots, \tilde{s}\}$, $\tilde{s} \leq n$, where $\rho: \{1, \dots, n\} \rightarrow \{1, \dots, n\}$ is a permutation on the sample indices $\{1, \dots, n\}$, it can be shown to have the form $\hat{\mu}_{KRR}^{\tilde{s}}(\mathbf{T} | \mathbf{x}_i) = \sum_{j=1}^{\tilde{s}} \beta_j(\mathbf{x}_i) \phi(\mathbf{t}_{\rho(j)})$ for some scalars $\beta_j(\mathbf{x}_i)$ [37].

We now pick an arbitrary subset of the dataset as the input into the error function E , say $\{(\mathbf{x}_{\xi(1)}, \mathbf{t}_{\xi(1)}, \mathbf{y}_{\xi(1)}), \dots, (\mathbf{x}_{\xi(s)}, \mathbf{t}_{\xi(s)}, \mathbf{y}_{\xi(s)})\}$, where like ρ , $\xi: \{1, \dots, n\} \rightarrow \{1, \dots, n\}$ is also a permutation on the sample indices $\{1, \dots, n\}$. Then any minimizer of the empirical risk applied to that subset

$$f^* = \arg \min_{f \in \mathcal{H}_k} \left\{ E \left[\left\{ (\mathbf{x}_{\xi(1)}, \mathbf{t}_{\xi(1)}), y - \zeta(\mathbf{x}_{\xi(1)}), \left\langle f, \psi(\mathbf{x}_{\xi(1)}) \otimes [\phi(\mathbf{t}_{\xi(1)}) - \hat{\mu}_{KRR}^{\tilde{s}}(\mathbf{T} | \mathbf{x}_{\xi(1)})] \right\rangle \right\}, \dots, \right. \right. \\ \left. \left. \left\{ (\mathbf{x}_{\xi(s)}, \mathbf{t}_{\xi(s)}), y - \zeta(\mathbf{x}_{\xi(s)}), \left\langle f, \psi(\mathbf{x}_{\xi(s)}) \otimes [\phi(\mathbf{t}_{\xi(s)}) - \hat{\mu}_{KRR}^{\xi(s)}(\mathbf{T} | \mathbf{x}_{\xi(s)})] \right\rangle \right\} \right] \right. \\ \left. + \Omega(\|f\|) \right\}$$

admits a representation of form $f^*(\mathbf{x}, \mathbf{t}) = \sum_{i=1}^n \alpha_{ij} k_{\mathcal{X}}(\mathbf{x}, \mathbf{x}_i) k_{\mathcal{T}}(\mathbf{t}, \mathbf{t}_j)$. Here, we leverage the isometric isomorphism between $\mathcal{H}_{\mathcal{X} \times \mathcal{T}}$ and $\mathcal{H}_{\mathcal{X}} \times \mathcal{H}_{\mathcal{T}}$ and write $k_{\mathcal{X} \times \mathcal{T}}((\mathbf{x}, \mathbf{t}), (\mathbf{x}', \mathbf{t}')) = k_{\mathcal{X}}(\mathbf{x}, \mathbf{x}') k_{\mathcal{T}}(\mathbf{t}, \mathbf{t}')$ where $k_{\mathcal{X}}$ and $k_{\mathcal{T}}$ are the kernels on $\mathcal{H}_{\mathcal{X}}$ and $\mathcal{H}_{\mathcal{T}}$ respectively.

Proof. Define mappings

$$\psi : \mathcal{X} \rightarrow \mathcal{H}_{\mathcal{X}} \quad (17)$$

$$x \mapsto k_{\mathcal{X}}(x, \cdot) \quad (18)$$

$$\phi : \mathcal{T} \rightarrow \mathcal{H}_{\mathcal{T}} \quad (19)$$

$$t \mapsto k_{\mathcal{T}}(t, \cdot) \quad (20)$$

Since $k_{\mathcal{X}}, k_{\mathcal{T}}$ are reproducing kernels, $\psi(x)(x') = k_{\mathcal{X}}(x, x') = \langle \psi(x), \psi(x') \rangle_{\mathcal{X}}$. Similarly $\phi(t)(t') = k_{\mathcal{T}}(t, t') = \langle \phi(t), \phi(t') \rangle_{\mathcal{T}}$. Given any $(x_1, t_1), \dots, (x_n, t_n)$, one can use orthogonal projection to decompose any $f \in \mathcal{H}_{\mathcal{X} \times \mathcal{T}}$ into the sum of two functions, one lying in the span $\{\psi(x_i) \otimes \phi(t_j) : i = 1, \dots, n, j = 1, \dots, n\}$ and the other lying in the orthogonal complement

$$f = \sum_{i,j=1}^n \alpha_{ij} \psi(x_i) \otimes \phi(t_i) + v, \quad (21)$$

$$\text{where } \langle v, \psi(x_i) \otimes \phi(t_j) \rangle_{\mathcal{H}_{\mathcal{X} \times \mathcal{T}}} = 0, \quad \forall i, j \in \{1, \dots, n\}.$$

Then f applied to any training point (x_k, t_k) gives

$$\langle f, \psi(x_k) \otimes \phi(t_k) \rangle_{\mathcal{H}_{\mathcal{X} \times \mathcal{T}}} = f(x_k, t_k) \quad (22)$$

$$= \left\langle \sum_{i,j=1}^n \alpha_{ij} \psi(x_i) \otimes \phi(t_j) + v, \psi(x_k) \otimes \phi(t_k) \right\rangle_{\mathcal{H}_{\mathcal{X} \times \mathcal{T}}} \quad (23)$$

$$= \sum_{i,j=1}^n \alpha_{ij} \langle \psi(x_i), \psi(x_k) \rangle_{\mathcal{H}_{\mathcal{X}}} \langle \phi(t_j), \phi(t_k) \rangle_{\mathcal{H}_{\mathcal{T}}}, \quad (24)$$

where we note that eq. (24) is independent of v .

Moreover, the conditional expectation of $f(\mathbf{X}, \mathbf{T})$ given training point $\mathbf{X} = \mathbf{x}_k$ is approximated as

$$\mathbb{E}[f(\mathbf{X}, \mathbf{T}) | \mathbf{X}] \approx \left\langle f, \psi(x_k) \otimes \hat{\mu}_{KRR}^{\tilde{s}} \right\rangle_{\mathcal{H}_{\mathcal{X} \times \mathcal{T}}} \quad (25)$$

$$= \left\langle \sum_{i,j=1}^n \alpha_{ij} \psi(x_i) \otimes \phi(t_j) + v, \psi(x_k) \otimes \hat{\mu}_{KRR}^{\tilde{s}} \right\rangle_{\mathcal{H}_{\mathcal{X} \times \mathcal{T}}} \quad (26)$$

$$= \left\langle \sum_{i,j=1}^n \alpha_{ij} \psi(x_i) \otimes \phi(t_j) + v, \psi(x_k) \otimes \sum_{j=1}^{\tilde{s}} \beta_j(x_k) \phi(t_{\rho(j)}) \right\rangle_{\mathcal{H}_{\mathcal{X} \times \mathcal{T}}} \quad (27)$$

$$= \left\langle \sum_{i,j=1}^n \alpha_{ij} \psi(x_i) \otimes \phi(t_j), \psi(x_k) \otimes \sum_{j=1}^{\tilde{s}} \beta_j(x_k) \phi(t_{\rho(j)}) \right\rangle_{\mathcal{H}_{\mathcal{X} \times \mathcal{T}}}, \quad (28)$$

where to get the last equality, we note that the second argument of the inner product lies in the orthogonal complement of v . Hence, the value of error E in eq. (17) is likewise independent of v .

Regarding the second (regularization) term, we use the fact that v is orthogonal to $\sum_{i,j=1}^n \alpha_{ij} \psi(\mathbf{x}_i) \otimes \phi(\mathbf{t}_j)$ and Ω is strictly increasing. Thus, we have

$$\Omega(\|f\|) = \Omega\left(\left\|\sum_{i,j=1}^n \alpha_{ij} \psi(\mathbf{x}_i) \otimes \phi(\mathbf{t}_j) + v\right\|\right) \quad (29)$$

$$= \Omega\left(\sqrt{\left\|\sum_{i,j=1}^n \alpha_{ij} \psi(\mathbf{x}_i) \otimes \phi(\mathbf{t}_j)\right\|^2 + \|v\|^2}\right) \quad (30)$$

$$\geq \Omega\left(\left\|\sum_{i,j=1}^n \alpha_{ij} \psi(\mathbf{x}_i) \otimes \phi(\mathbf{t}_j)\right\|\right). \quad (31)$$

Therefore, setting $v = 0$ does not affect the first term of the error function, but it does not increase the second term, so the minimizer \hat{f} must be of the form

$$\hat{f}(\mathbf{x}, \mathbf{t}) = \sum_{i,j=1}^n \alpha_{ij} \langle \psi(\mathbf{x}), \psi(\mathbf{x}_i) \rangle_{\mathcal{H}_{\mathcal{X}}} \langle \phi(\mathbf{t}), \phi(\mathbf{t}_j) \rangle_{\mathcal{H}_{\mathcal{T}}} \quad (32)$$

$$= \sum_{i,j=1}^n \alpha_{ij} k_{\mathcal{X}}(\mathbf{x}, \mathbf{x}_i) k_{\mathcal{T}}(\mathbf{t}, \mathbf{t}_j). \quad (33)$$

□

Proof of Proposition 1 (Universality of product effect) Having established a necessary extension of the Representer Theorem in Lemma 2, we now prove the universality of our proposed product effect condition. This proposition implies that we may approximate any bounded continuous function in $\mathcal{C}(\mathcal{X} \times \mathcal{T})$, given enough dimensions for g and h .

Proof. Suppose \tilde{N} is the total number of data points available to us. First we restate the empirical loss function:

$$\hat{f} = \arg \min_{f \in \mathcal{F}} \frac{1}{N} \sum_{i=1}^N \left[\{y_i - \hat{m}(\mathbf{x}_i)\} - (f(\mathbf{x}_i, \mathbf{t}_i) - \hat{e}^p(\mathbf{x}_i)) \right]^2 + \Omega(\|f\|_{\mathcal{H}_{\mathcal{X} \times \mathcal{T}}}). \quad (34)$$

where $N \leq \tilde{N}$, and Ω is any strictly increasing function acting as the regularizer.

Inheriting the notation of Lemma 2, set

- $n = \tilde{N}$
- $s = N$ to be the size of the sample used to compute the empirical loss eq. (34).
- $\zeta(\mathbf{x}) = \hat{m}(\mathbf{x})$
- $\tilde{s} \leq \tilde{N}$ be the size of sample used to obtain $\hat{\mu}_{KRR}^{\tilde{s}}(\mathbf{T} | \mathbf{X})$, hence

$$\begin{aligned} \hat{e}^p(\mathbf{x}_i) &= \langle f, \psi(\mathbf{x}) \otimes \hat{\mu}_{KRR}^{\tilde{s}}(\mathbf{T} | \mathbf{X}) \rangle \approx \langle f, \psi(\mathbf{x}) \otimes \mu(\mathbf{T} | \mathbf{X}) \rangle_{\mathcal{H}_{\mathcal{X} \times \mathcal{T}}} \\ &= \mathbb{E}[f(\mathbf{X}, \mathbf{T}) | \mathbf{X}] \end{aligned} \quad (35)$$

Then, by applying Lemma 2, we know that the minimizer \hat{f} has the form

$$\hat{f}(\mathbf{x}, \mathbf{t}) = \sum_{i,j=1}^n \alpha_{ij} k_{\mathcal{X}}(\mathbf{x}_i, \mathbf{x}) k_{\mathcal{T}}(\mathbf{t}_j, \mathbf{t}) \quad (36)$$

Flattening this double sum gives

$$\hat{f}(\mathbf{x}, \mathbf{t}) = \sum_{l=1}^n \alpha_{\pi(l)\omega(l)} k_{\mathcal{X}}(\mathbf{x}_{\pi(l)}, \mathbf{x}) k_{\mathcal{T}}(\mathbf{t}_{\omega(l)}, \mathbf{t}), \quad \pi(l) = \lceil l/n \rceil, \quad \omega(l) = l \bmod n \quad (37)$$

Then, we may recover $f(\mathbf{x}, \mathbf{t}) = \langle g(\mathbf{x}), h(\mathbf{t}) \rangle$ by defining

$$g(\mathbf{x}) = \begin{pmatrix} \sqrt{\alpha_{\pi(1)\omega(1)}} k_{\mathcal{X}}(\mathbf{x}_{\pi(1)}, \mathbf{x}) \\ \vdots \\ \sqrt{\alpha_{\pi(n)\omega(n)}} k_{\mathcal{X}}(\mathbf{x}_{\pi(n)}, \mathbf{x}) \end{pmatrix} \quad h(\mathbf{t}) = \begin{pmatrix} \sqrt{\alpha_{\pi(1)\omega(1)}} k_{\mathcal{T}}(\mathbf{t}_{\omega(1)}, \mathbf{t}) \\ \vdots \\ \sqrt{\alpha_{\pi(n)\omega(n)}} k_{\mathcal{T}}(\mathbf{t}_{\omega(n)}, \mathbf{t}) \end{pmatrix} \quad (38)$$

□

Finally, by choosing universal kernels on $\mathcal{H}_{\mathcal{X}}$ and $\mathcal{H}_{\mathcal{T}}$, $\mathcal{H}_{\mathcal{X}} \times \mathcal{H}_{\mathcal{T}}$ is dense in $\mathcal{C}(\mathcal{X} \times \mathcal{T})$, and we may approximate arbitrary continuous functions in $\mathcal{C}(\mathcal{X} \times \mathcal{T})$. Note that the dimensionality of g and h grows with the number of samples, and in practice are chosen as a hyperparameter. Although this decomposition is not unique, for our purpose it is sufficient because we only require the representation $g(\mathbf{x})^\top h(\mathbf{t})$ to be sufficiently expressive in order to approximate any bounded continuous function which acts as the model for $\mathbb{E}[Y | \mathbf{X} = \mathbf{x}, \mathbf{T} = \mathbf{t}]$.

Remark 1. (Cross-fitting) Note that we assumed a 2-stage Kernel Ridge Regression estimator for the kernel condition mean embedding $\mu(\mathbf{T} | \mathbf{X})$. Analogously, one may extend Lemma 2 to the case where we fit the conditional mean embeddings $\mu_i(\mathbf{T} | \mathbf{X})$, $i \in \{1, \dots, N\}$, through cross-fitting.

B Derivation of Robinson Decomposition for Product Effects

We consider the following partial parameterization of $p(y | \mathbf{x}, \mathbf{t})$,

$$Y = \underbrace{g(\mathbf{X})^\top h(\mathbf{T})}_{=: f(\mathbf{X}, \mathbf{T})} + \varepsilon, \quad (39)$$

where $g : \mathcal{X} \rightarrow \mathbb{R}^d$, $h : \mathcal{T} \rightarrow \mathbb{R}^d$ and $\mathbb{E}[\varepsilon | \mathbf{x}, \mathbf{t}] = \mathbb{E}[\varepsilon | \mathbf{x}] = 0$, for all $(\mathbf{x}, \mathbf{t}) \in \mathcal{X} \times \mathcal{T}$. Rearranging eq. (39) yields the Robinson residual

$$\varepsilon = Y - g(\mathbf{X})^\top h(\mathbf{T}), \quad (40)$$

which we aim to rewrite in terms of $m(\mathbf{X})$. To this end, we define *propensity features* $e^h(\mathbf{X})$ as

$$e^h(\mathbf{X}) \triangleq \mathbb{E}[h(\mathbf{T}) | \mathbf{X}], \quad \text{such that} \quad m(\mathbf{X}) = \mathbb{E}[Y | \mathbf{X}] = g(\mathbf{X})^\top e^h(\mathbf{X}). \quad (41)$$

To obtain the generalized Robinson decomposition, one rewrites eq. (40) as

$$\varepsilon = Y - \left(g(\mathbf{X})^\top \left[h(\mathbf{T}) + e^h(\mathbf{X}) - \cancel{e^h(\mathbf{X})} \right] \right) \quad (42)$$

$$= Y - \left(g(\mathbf{X})^\top e^h(\mathbf{X}) + g(\mathbf{X})^\top (h(\mathbf{T}) - e^h(\mathbf{X})) \right) \quad (43)$$

$$= Y - \underbrace{\left(g(\mathbf{X})^\top e^h(\mathbf{X}) \right)}_{m(\mathbf{X})} - g(\mathbf{X})^\top (h(\mathbf{T}) - e^h(\mathbf{X})). \quad (44)$$

Hence, the generalized Robinson decomposition for product effects is

$$Y - m(\mathbf{X}) = g(\mathbf{X})^\top (h(\mathbf{T}) - e^h(\mathbf{X})) + \varepsilon. \quad (45)$$

C Experimental Details

C.1 Simulations

Baseline effect Similarly as in [7, 11, 42], for each run of the experiment, we randomly sample a vector $\mathbf{u}_0 \sim \mathcal{U}(\mathbf{0}, \mathbf{1})$, and set $\mathbf{v}_0 = \mathbf{u}_0 / \|\mathbf{u}_0\|$ where $\|\cdot\|$ is the Euclidean norm. We then model the baseline effect as

$$\mu_0(\mathbf{x}) = \mathbf{v}_0^\top \mathbf{x}. \quad (46)$$

C.1.1 Small-World Networks

Covariates We uniformly sample 20-dimensional multivariate covariates $\mathbf{X} \sim \mathcal{U}(-1, 1)$. The in-sample dataset consists of 1,000 units, and the out-sample one of 500. For the treatment assignment, we square the covariates element-wise; i.e., we sample treatment assignments according to $p(\mathbf{T} | \mathbf{x}^2)$.

Graph interventions For each graph intervention, we uniformly sample a number of nodes between 10 and 120, number of neighbors for each node between 3 and 8, and the probability of rewiring each edge between 0.1 and 1. Then, we repeatedly generate Watts–Strogatz small-world graphs until we get a connected one. Each vertex has one feature, which is its degree centrality. We denote a graph’s node connectivity as $\nu(\mathcal{G})$ and its average shortest path length as $l(\mathcal{G})$.

Outcomes Analogously as for the baseline effect, we generate two randomly sampled vectors \mathbf{v}_ν and \mathbf{v}_l . Then, given an assigned graph treatment \mathcal{G} and a covariate vector \mathbf{x} , we generate the outcome as

$$Y = 100\mu_0(\mathbf{x}) + 0.2\nu(\mathcal{G})^2 \cdot \mathbf{v}_\nu^\top \mathbf{x} + l(\mathcal{G}) \cdot \mathbf{v}_l^\top \mathbf{x} + \epsilon, \quad \epsilon \sim \mathcal{N}(0, 1). \quad (47)$$

C.1.2 TCGA

Covariates The *The Cancer Genomic Atlas* (TCGA) simulation uses 4,000-dimensional 9,659 gene expression measurements of cancer patients for covariates [63], i.e., each unit is a covariate vector $\mathbf{X} \in \mathbb{R}^{4000}$. The in-sample and out-sample datasets consist of 5,000 and 4,659 units, respectively. In each run, the units are split randomly into in- and out-sample datasets. We used the same version of the TCGA dataset as used by Bica et al. [7] and Schwab et al. [52].

Graph interventions In each run, we randomly sample 10,000 molecules from the Quantum Machine 9 (QM9) dataset [46, 49] (with 133k molecules in total). For each molecule, we create a relational graph, where each node corresponds to an atom and consists of 78 atom features. An edge corresponds to the chemical bond type, where we label each edge correspondingly, considering *single*, *double*, *triple* and *aromatic* bonds. Furthermore, for each molecule, we obtain 8 of its properties *mu*, *alpha*, *homo*, *lumo*, *gap*, *r2*, *zpve*, *u0*, which we collect in the vector $\mathbf{z} \in \mathbb{R}^8$.

Outcomes For each covariate vector \mathbf{x} , we compute its 8-dimensional PCA components, denoted by $\mathbf{x}^{(\text{PCA})} \in \mathbb{R}^8$. Then, given the molecular properties of the assigned molecule treatment \mathbf{z} , we generate outcomes by

$$Y = 10\mu_0(\mathbf{x}) + 0.01\mathbf{z}^\top \mathbf{x}^{(\text{PCA})} + \epsilon, \quad \epsilon \sim \mathcal{N}(0, 1). \quad (48)$$

C.2 Hyper-parameters

To ensure a fair comparison between all models, we perform hyper-parameter optimization with random search for all models on held-out data and select the best hyper-parameters over 10 runs. While conceptually, choosing hyper-parameters based on predictive metrics may not necessarily lead to good CATE estimation performance, Neal et al. [41] provide empirical evidence that doing so indeed often does in practice.

Table 2 and Table 4 include the hyper-parameter search ranges we set in the SW and TCGA experiments, respectively. Table 3 and Table 5 include the fixed hyper-parameter values across all SW and TCGA experiments, respectively. We restricted the number of hyper-parameter optimization

trials to 10 in all experiments. We observed that all models' performances are rather insensitive to hyper-parameter values in the considered search ranges, i.e., the performances across trials have not varied much. The search ranges for the HSIC penalty λ are taken from the experimental section of the GraphITE paper [18], where the authors also argue that their model's performance is insensitive to this weight. In consultation with Harada & Kashima [18], we use Ma et al. [36]'s implementation of the normalized HSIC. We use early stopping for all models based on their training loss. We noticed that a patience value below 10 often leads to pre-convergence stopping with subsequent sub-optimal performance for all models but GIN.

C.2.1 SW

Hyper-parameter	Search range
Num. of layers for covariates representations	2-4
Num. of layers for treatment representations	3-6
Num. of layers for $\hat{m}_\theta(\mathbf{X})^*$	3-6
Num. of layers for $\hat{e}_\eta^h(\mathbf{X})^*$	3-6
Num. of layer for final feed-forward network †	2-6
Dim. of hidden layers for covariates representations	50-300
Dim. of hidden layers for treatment representations	50-300
Dim. of hidden layers for $\hat{m}_\theta(\mathbf{X})^*$	200-300
Dim. of hidden layers for $\hat{e}_\eta^h(\mathbf{X})^*$	50-150
Dim. of $\hat{g}_\psi(\mathbf{X}), \hat{h}_\phi(\mathbf{T})^*$	50-250
Dim. of final covariates/treatment layer	2-200
Dim. of hidden layers for final feed-forward network	50-300
Num. update steps K^*	10-20
Early stopping patience for $\hat{m}_\theta(\mathbf{X})^*$	{5, 10}
Early stopping patience for $\hat{g}_\psi(\mathbf{X}), \hat{h}_\phi(\mathbf{T}), \hat{e}_\eta^h(\mathbf{X})^*$	{1, 5}
Learning rates $\lambda_\psi, \lambda_\phi^*$	{5e-4, 1e-3}
Learning rate †	{5e-4, 1e-3}
Dropout for $\hat{m}_\theta(\mathbf{X})^*$	{0, 0.2}
Dropout for $\hat{e}_\eta^h(\mathbf{X})^*$	{0, 0.2}
Weight of HSIC penalty λ^\ddagger	{0.001, 0.01, 1, 10, 100, 1000}

Table 2: Hyper-parameter search ranges for SW experiments. * denotes hyper-parameter only applicable for GIN; † applicable for all models but GIN, ‡ applicable only for GraphITE.

Hyper-parameter	Value
Optimizer	Adam [30]
Batch size	500
Weight decay (all optims.)	0
$\lambda_\theta, \lambda_\eta$	1e-3
Early stopping patience †	10
GNN Batch Norm	True
MLP Batch Norm (all MLPs)	False
Activation functions (all layers)	ReLU
Validation set size (in %)	20%

Table 3: Fixed hyper-parameter values across all SW experiments. * denotes hyper-parameter only applicable for GIN; † applicable for all models but GIN, ‡ applicable only for GraphITE.

C.2.2 TCGA

Hyper-parameter	Search range
Num. of layers for covariates representations	2-5
Num. of layers for treatment representations	3-6
Num. of layers for $\hat{m}_\theta(\mathbf{X})^*$	2-4
Num. of layers for $\hat{e}_\eta^h(\mathbf{X})^*$	1-6
Num. of layer for final feed-forward network †	1-5
Dim. of hidden layers for covariates representations	100-400
Dim. of hidden layers for treatment representations	100-400
Dim. of hidden layers for $\hat{m}_\theta(\mathbf{X})^*$	100-300
Dim. of hidden layers for $\hat{e}_\eta^h(\mathbf{X})^*$	10-50
Dim. of $\hat{g}_\psi(\mathbf{X}), \hat{h}_\phi(\mathbf{T})^*$	200-600
Dim. of final covariates/treatment layer	2-800
Dim. of hidden layers for final feed-forward network	100-400
Num. update steps K^*	10-20
Early stopping patience for $\hat{g}_\psi(\mathbf{X}), \hat{h}_\phi(\mathbf{T}), \hat{e}_\eta^h(\mathbf{X})^*$	{5, 10}
Learning rates $\lambda_\psi, \lambda_\phi^*$	{5e-4, 1e-3}
Learning rate †	{5e-4, 1e-3}
Weight of HSIC penalty λ^\ddagger	{0.001, 0.01, 1, 10, 100, 1000}

Table 4: Hyper-parameter search ranges for TCGA experiments. * denotes hyper-parameter only applicable for GIN; † applicable for all models but GIN, ‡ applicable only for GraphITE.

Hyper-parameter	Value
Optimizer	Adam [30]
Batch size	1000
Weight decay (all optims.)	0
$\lambda_\theta, \lambda_\eta$	1e-3
Early stopping patience †	10
GNN Batch Norm	True
MLP Batch Norm (all MLPs)	False
Activation functions (all layers)	ReLU
Validation set size (in %)	20%

Table 5: Fixed hyper-parameter values across all TCGA experiments. * denotes hyper-parameter only applicable for GIN; † applicable for all models but GIN, ‡ applicable only for GraphITE.

C.2.3 Hardware details

All experiments were run on Microsoft Azure Virtual Machines with 12 Intel Xeon E5-2690 v4 CPUs and 2 NVIDIA Tesla K80 GPUs. No single trial took longer than ~ 30 minutes to run.

D Additional Results

D.1 Comparison of Performances on different K Treatments

We present additional WPEHE@ K results for the experiments in Section 5.2 with varying K .

Method	SW		TCGA	
	In-sample	Out-sample	In-sample	Out-sample
WPEHE@2				
Zero	52.17 \pm 7.37	41.36 \pm 5.04	25.17 \pm 8.12	17.33 \pm 5.41
CAT	44.63 \pm 8.18	37.65 \pm 5.90	160.35 \pm 58.56	149.75 \pm 46.86
GNN	32.98 \pm 6.63	26.47 \pm 3.87	29.35 \pm 8.90	27.17 \pm 8.67
GraphITE	30.18 \pm 6.45	25.39 \pm 4.04	28.60 \pm 9.44	27.37 \pm 9.87
GIN	18.00 \pm 3.83	15.30 \pm 2.60	10.44 \pm 3.62	7.76 \pm 1.56
WPEHE@3				
Zero	51.61 \pm 7.24	41.53 \pm 4.96	25.97 \pm 7.96	17.50 \pm 5.11
CAT	44.87 \pm 7.53	37.59 \pm 5.46	159.48 \pm 56.46	148.80 \pm 44.87
GNN	32.97 \pm 5.75	26.60 \pm 3.70	30.22 \pm 8.77	27.29 \pm 8.30
GraphITE	30.39 \pm 5.89	25.70 \pm 3.70	29.71 \pm 9.43	27.27 \pm 9.38
GIN	19.79 \pm 4.06	15.54 \pm 2.56	10.62 \pm 3.56	7.94 \pm 1.51
WPEHE@4				
Zero	52.92 \pm 7.47	47.93 \pm 6.68	26.35 \pm 7.79	17.76 \pm 5.05
CAT	46.95 \pm 7.65	42.47 \pm 6.91	158.02 \pm 54.76	148.08 \pm 43.71
GNN	33.89 \pm 5.73	31.51 \pm 5.27	30.51 \pm 8.57	27.53 \pm 8.23
GraphITE	31.43 \pm 5.75	30.39 \pm 5.71	30.07 \pm 9.22	27.48 \pm 9.28
GIN	20.78 \pm 4.11	19.50 \pm 4.12	10.76 \pm 3.51	8.08 \pm 1.51
WPEHE@5				
Zero	55.02 \pm 8.00	50.75 \pm 7.92	26.53 \pm 7.66	17.91 \pm 4.96
CAT	49.78 \pm 8.37	46.65 \pm 8.86	156.77 \pm 53.58	147.20 \pm 42.86
GNN	36.06 \pm 6.69	34.16 \pm 6.41	30.61 \pm 8.41	27.61 \pm 8.10
GraphITE	33.69 \pm 6.56	33.13 \pm 6.92	30.22 \pm 9.08	27.53 \pm 9.12
GIN	22.06 \pm 4.40	21.19 \pm 4.80	10.90 \pm 3.47	8.13 \pm 1.49
WPEHE@6				
Zero	56.26 \pm 8.12	53.77 \pm 8.93	26.63 \pm 7.55	17.94 \pm 4.86
CAT	51.75 \pm 8.85	49.76 \pm 9.73	155.88 \pm 52.82	146.62 \pm 42.32
GNN	37.10 \pm 6.84	36.74 \pm 7.42	30.67 \pm 8.29	27.57 \pm 7.95
GraphITE	34.81 \pm 6.70	35.94 \pm 8.07	30.31 \pm 8.96	27.48 \pm 8.95
GIN	23.00 \pm 4.56	23.19 \pm 5.56	10.98 \pm 3.45	8.15 \pm 1.46
WPEHE@7				
Zero	58.16 \pm 8.38	55.73 \pm 9.01	26.66 \pm 7.48	17.97 \pm 4.81
CAT	54.62 \pm 9.27	52.21 \pm 9.74	155.24 \pm 52.25	146.15 \pm 41.90
GNN	39.21 \pm 7.05	38.51 \pm 7.50	30.67 \pm 8.21	27.56 \pm 7.86
GraphITE	37.00 \pm 7.10	37.34 \pm 8.05	30.33 \pm 8.88	27.47 \pm 8.86
GIN	24.71 \pm 5.07	24.46 \pm 5.79	11.02 \pm 3.43	8.17 \pm 1.45
WPEHE@8				
Zero	59.57 \pm 8.74	56.61 \pm 8.94	26.73 \pm 7.43	18.03 \pm 4.76
CAT	56.24 \pm 9.71	53.33 \pm 9.71	154.86 \pm 51.85	145.94 \pm 41.61
GNN	40.44 \pm 7.36	39.04 \pm 7.33	30.72 \pm 8.16	27.49 \pm 8.78
GraphITE	38.42 \pm 7.46	38.06 \pm 7.89	30.39 \pm 8.82	27.49 \pm 8.78
GIN	25.90 \pm 5.51	25.63 \pm 6.03	11.10 \pm 3.43	8.20 \pm 1.44
WPEHE@9				

Zero	60.39 ± 8.94	55.72 ± 8.44	26.75 ± 7.40	18.06 ± 4.73
CAT	57.78 ± 10.27	53.06 ± 9.36	154.60 ± 51.57	145.73 ± 41.37
GNN	41.45 ± 7.60	38.47 ± 6.92	30.72 ± 8.11	27.60 ± 7.74
GraphITE	39.43 ± 7.69	37.43 ± 7.48	30.39 ± 8.78	27.50 ± 8.72
GIN	26.76 ± 5.80	25.30 ± 5.75	11.12 ± 3.42	8.22 ± 1.43

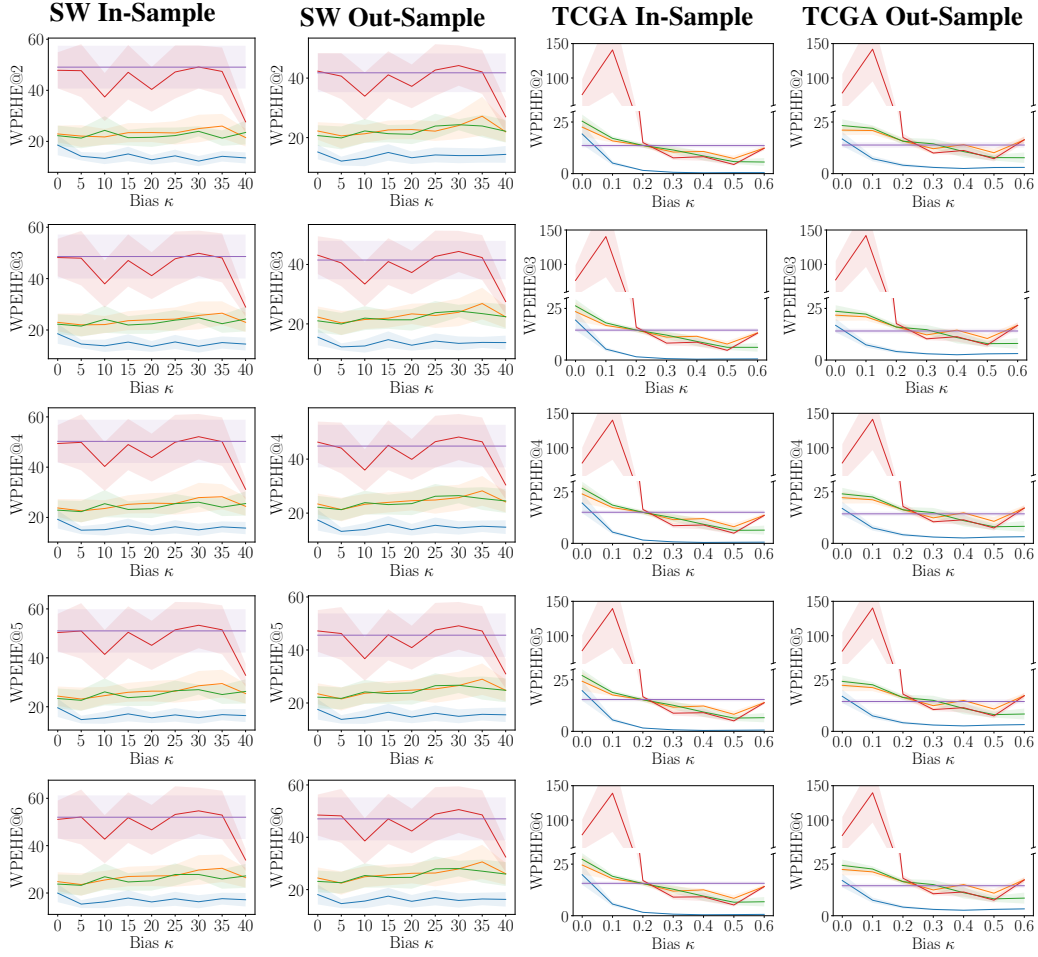
WPEHE@10

Zero	60.92 ± 9.10	56.44 ± 8.91	26.78 ± 7.35	18.09 ± 4.71
CAT	58.32 ± 10.29	54.76 ± 10.56	154.39 ± 51.32	145.57 ± 41.21
GNN	42.08 ± 7.82	39.11 ± 7.24	30.73 ± 8.07	27.61 ± 7.70
GraphITE	40.26 ± 7.94	37.99 ± 7.80	30.41 ± 8.74	27.51 ± 8.69
GIN	27.47 ± 6.07	26.01 ± 6.06	11.13 ± 3.41	8.23 ± 1.43

Table 6: Error of CATE estimation for all methods, measured by WPEHE@1 – 10. Results are averaged over 10 trials, \pm denotes std. error.

D.2 Comparison of Robustness to different Bias Strengths κ

We present additional WPEHE@ K results for the experiments in Section 5.3 over increasing bias strength κ and varying K .



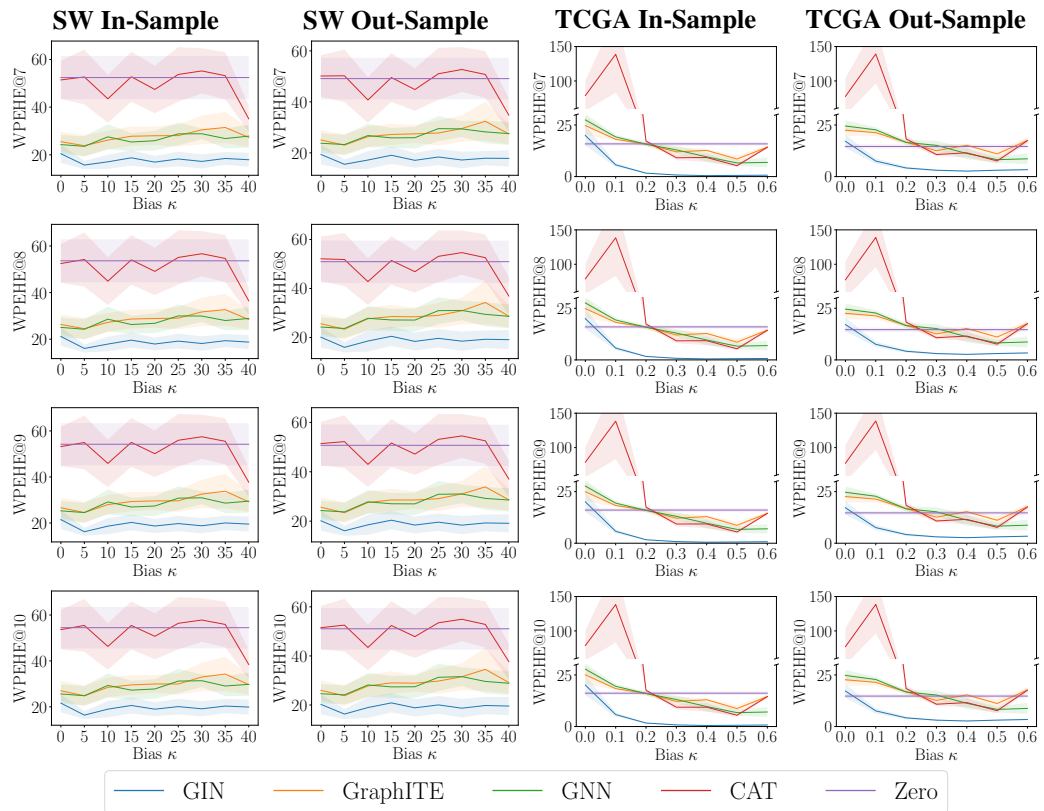


Figure 5: WPEHE@ K over increasing bias strength κ and varying K .